Article

Conformational Flip of Nonactivated HCN2 Channel Subunits Evoked by Cyclic Nucleotides

Susanne Thon,[1] Eckhard Schulz,[2] Jana Kusch,[1] and Klaus Benndorf[1,*]
[1]Institut für Physiologie II, Universitätsklinikum Jena, Jena, Germany; and [2]Fachhochschule Schmalkalden, Fakultät Elektrotechnik, Blechhammer, Schmalkalden, Germany

ABSTRACT Hyperpolarization-activated cyclic nucleotide-modulated (HCN) channels are tetrameric proteins that evoke electrical rhythmicity in specialized neurons and cardiomyocytes. The channels are activated by hyperpolarizing voltage but are also receptors for the intracellular ligand adenosine-3′,5′-cyclic monophosphate (cAMP) that enhances activation but is unable to activate the channels alone. Using fcAMP, a fluorescent derivative of cAMP, we analyzed the effect of ligand binding on HCN2 channels not preactivated by voltage. We identified a conformational flip of the channel as an intermediate state following the ligand binding and quantified it kinetically. Globally fitting the time courses of ligand binding and unbinding revealed modest cooperativity among the subunits in the conformational flip. The intensity of this cooperativity, however, was only moderate compared to channels preactivated by hyperpolarizing voltage. These data provide kinetic information about conformational changes proceeding in nonactivated HCN2 channels when cAMP binds. Moreover, our approach bears potential for analyzing the function of any other membrane receptor if a potent fluorescent ligand is available.

INTRODUCTION

The activity of hyperpolarization-activated cyclic nucleotide-modulated (HCN) pacemaker channels (1–3) evokes electrical rhythmicity in various types of brain neurons (4–11) and specialized heart cells (12–15). The channels are primarily activated by hyperpolarization of the membrane voltage (16,17). In addition to this, the second messenger adenosine-3′,5′-cyclic monophosphate (cAMP), produced upon sympathetic stimulation, can bind to the channels and further enhance activation (18–22), resulting in an acceleration of the electrical rhythm (7–10).

Structurally, HCN channels are tetramers. In mammals, four closely related genes, HCN1–HCN4, encode four homolog subunits (17,23) in which each contains a cyclic-nucleotide binding domain (CNBD) in its C-terminus (24). When expressed heterologously, all four isoforms can form functional homotetrameric channels (2,3,5,13,25).

The mechanism underlying the activation of HCN channels by voltage is poorly understood. The usage of voltage-clamp fluorometry in related spHCN channels provided the surprising result that the activation of only two of the available four subunits suffices to fully open the channels (26). When activating HCN channels in the presence of cAMP, the activation time course becomes accelerated and steady-state activation is shifted to less negative voltages, indicative of an intimate coupling between voltage- and ligand-induced activation. Experiments with channels formed by concatenated subunits containing a variable number of disabled binding sites suggest that in channels preactivated by voltage, all four subunits are involved in the generation of maximum activation (27). To quantify the dual gating of HCN channels, a cubic model has been proposed in which the voltage-independent closed-open transition is intimately coupled to a voltage step and a cAMP binding step (24,28). However, the degree of simplification in such a cubic model is a priori high because it ignores the tetrameric structure of the channels.

For ligand-induced activation of HCN2 channels preactivated by hyperpolarizing voltage, we recently substantiated a Markovian model that contains four binding steps and closed-open isomerizations from each of the five available closed states (29). Notably, the equilibrium association constants for the four binding steps, i.e., the microscopic affinity, reveals a cooperativity sequence of "positive-negative-positive" for the second, third, and fourth binding step, respectively (29). This cooperativity sequence differs fundamentally from the exclusively positive cooperativity for the four oxygen molecules binding to hemoglobin, probably the best-studied allosteric protein of all (for review, see Perutz et al. (30)). Consequently, Monod-Wyman-Changeux (MWC) models (31), with a constant allosteric factor used to describe the oxygen binding to hemoglobin, are invalid to describe the ligand-induced gating in HCN2 channels. Our previous analysis also showed that in HCN2 channels, preactivated by voltage, channel conformations with four, two, or zero ligands bound are more stable compared to channel conformations with either three ligands or one

Submitted January 15, 2015, and accepted for publication August 24, 2015.

*Correspondence: klaus.benndorf@mti.uni-jena.de

Editor: Miriam Goodman.

0006-3495/15/12/2268/9

http://dx.doi.org/10.1016/j.bpj.2015.08.054

ligand bound (29,32). This detailed insight into the gating of HCN2 channels was enabled by using confocal patch-clamp fluorometry (33) and jumps of a fluorescent cAMP (fcAMP) (29,34).

Our previous analyses also showed that not only HCN2 channels preactivated by a hyperpolarizing voltage pulse bind fcAMP, but also nonactivated channels at the voltage of −30 mV (34) and that channel activation enhances the overall affinity at the binding sites of the HCN2 channels by a factor of three, which was affirmed later by an alternative approach (35). However, the mechanism of binding in nonactivated channels has not been elucidated so far. In particular it is unanswered whether in nonactivated HCN2 channels the ligands bind independently or in a cooperative manner by interacting the subunits. It is also unknown how high the rates of binding and unbinding to the subunits are and how they differ from the values of a preactivated channel, and whether or not there are rate-limiting conformational changes associated with the ligand binding.

Herein we applied confocal patch-clamp fluorometry with jumps of the fcAMP concentration to nonactivated HCN2 channels. Analyzing time courses of ligand binding and unbinding and the steady-state concentration-binding relationship by Markovian models allowed us to identify a conformational flip (36,37) of the channel after the ligand binding and to quantify the kinetics of this flip. Furthermore, we quantified the interaction of the subunits, which was less pronounced compared to channels preactivated by hyperpolarizing voltage.

MATERIALS AND METHODS

Oocyte preparation and cRNA injection

Oocytes were obtained surgically under anesthesia (0.3% 3-aminobenzoic acid ethyl ester) from adult females of *Xenopus leavis* as described in Thon et al. (38).

Confocal patch-clamp fluorometry

Experiments were performed in inside-out macropatches of *Xenopus laevis* oocytes expressing homotetrameric HCN2 channels of the mouse (NM_008226) (34). All measurements were started 3.5 min after patch excision to minimize run down phenomena. The bath solution contained 100 mM KCl, 10 mM EGTA, and 10 mM HEPES (pH 7.2). The pipette solution contained 120 mM KCl, 10 mM HEPES, and 1.0 mM $CaCl_2$ (pH 7.2). Jumps of the ligand concentration (from zero to either 0.075, 0.25, 0.75, 2.5, or 7.5 μM, and back to zero) were performed by a double-barreled θ-glass pipette mounted on a piezo-driven device (39). The recording rate of our images was 10 Hz for recording the time courses and either 8.3 or 10 Hz for determining the steady-state values. The solution exchange at the pipette tip was completed within 1 ms. At the very membrane patch inside the pipette, the solution exchange is slowed by additional diffusion within the confined volume and effects of cytosolic cell material sticking at the patch. In the time courses analyzed herein, the solution exchange was shorter than 100 ms, the duration for one frame. Current recording was performed with the ISO3 hard- and software (MFK, Niedernhausen, Germany; sampling rate 200 Hz, 4-pole Bessel filter set to 2 kHz).

The fluorescence intensity in the patch was measured by patch-clamp fluorometry (40) combined with confocal microscopy. The method has been described in detail previously (33). As fluorescent ligand we used 8-DY547-AET-cAMP (fcAMP) (29,34). Recording was performed with the confocal microscope LSM 710 (Zeiss, Jena, Germany). All fluorescence signals were normalized with respect to the maximum fluorescence, F_{max}, determined at the voltage of −130 mV in the presence of the saturating fcAMP concentration of 15 μM.

To exclude that fcAMP binds to hypothetical additional binding sites outside the CNBD, eventually distorting our data, we performed control experiments with HCN2 channels in which a point mutation in the CNBD (R591E) generates a decrease of the apparent affinity for cAMP by more than three orders of magnitude (19,27). Functional expression of HCN2(R591E) channels was tested by voltage steps to −130 mV. With the saturating fcAMP concentration of 15 μM we obtained at −30 mV 0.9 ± 0.8 a.u. ($n = 5$) for patches from oocytes injected with HCN2(R591E) and 5.0 ± 1.2 a.u. ($n = 4$) for patches from water-injected oocytes. Both values are much smaller than the mean fluorescence of 34.7 ± 5.4 a.u. ($n = 8$) obtained for HCN2 channels. These experiments rule out any binding of fcAMP to additional binding sites outside the CNBD.

Data analysis

Steady-state concentration-binding relationships were fitted by

$$F/F_{max} = 1/\left(1 + (BC_{50}/[\text{fcAMP}])^{H}\right), \quad (1)$$

where F is the actual fluorescence, F_{max} the maximum fluorescence at −130 mV and 15 μM fcAMP. BC_{50} is the fcAMP concentration generating the half-maximum binding and H is the Hill coefficient. The time courses of ligand binding and unbinding were fitted according to

$$F/F_{max} = A[1 - \exp(-t/\tau_b)], \quad (2a)$$

$$F/F_{max} = A\exp(-t/\tau_u), \quad (2b)$$

where τ_b and τ_u are the time constants of binding and unbinding, respectively. The value A is a scaling factor and t is the time.

Data are shown as mean ± SE. Fits of equations to data points were performed with the software Origin8 (Northampton, MA).

Fitting Markovian models

The rate and/or equilibrium constants for Markovian models were obtained by globally fitting normalized averaged time courses of fcAMP binding and unbinding, following concentration jumps, and the respective steady-state values of binding. When building averaged time courses, each individual trace was considered to contribute with the same weight, i.e., the different number of channels in the patch was not considered. To determine the rate constants for a given model, the averaged and normalized time courses of binding/unbinding at 0.075, 0.25, 0.75, 2.5, and 7.5 μM fcAMP were subjected to a global fit together with the steady-state values at the same concentrations and one additional concentration of 15 μM, using a modified Levenberg-Marquardt algorithm (41,42). The approach is essentially the same as that reported earlier (29,33).

In brief: the goodness of the fit was judged by determining the χ^2 value from the fitted curves,

$$\chi^2 = g\left[\sum_{i=1}^{n_t}\sum_{j=1}^{n_d}\frac{\left(F_m(t_j,x_i) - F_c(t_j,x_i)\right)^2}{\sigma_F^2(t_j,x_i)}\right] + \sum_{i=1}^{n_s}\frac{(Bi_m(x_i)) - (Bi_c(x_i))^2}{\sigma_{Bi}^2(x_i)}, \quad (3)$$

where $F_m(t_j,x_i)$ are mean fluorescence values, measured at time t_j ($n_d = 60$) and concentration x_i ($n_t = 5$) and normalized to the maximum value at the end of the activation interval. $F_c(t_j,x_i)$ are the corresponding data points calculated by the fit. The square of the deviations at time t_j and concentration x_i was weighted by the reciprocal values of the observed variance $\sigma^2{}_F$ (t_j, x_i) calculated from the set of the normalized individual traces. $Bi_m(x_i)$ are the steady-state values of the normalized fluorescence intensity (degree of binding) at the concentration x_i ($n_s = 6$), and $Bi_c(x_i)$ are the respective calculated data points. Also the squared deviations of these steady-state values were weighted by the variance $\sigma^2{}_{Bi}$ (x_i). Because in the time courses the number of points to be fitted is n_d-times bigger than those in the steady-state relationships, we employed the factor $g = n_s/(n_t\, n_d) = 0.02$ to give the time courses and the steady-state relationships the same weight in the fit.

To calculate the data points of the time courses for the fit, the differential equation

$$d\mathbf{p}(t,x)/dt \;=\; \mathbf{p}(t,x)\mathbf{Q}(x) \tag{4}$$

was solved with the eigenvalue method. Here $\mathbf{Q}(x)$ is the $\mathbf{Q}$-matrix depending on the concentration x and $\mathbf{p}(t, x)$ is the row-vector of the probabilities to be in one of the states of the model (43). It should be noted that for a given concentration profile equation, Eq. 4 has to be solved for each pulse separately.

The steady-state values $\mathbf{p}(\infty, x_i)$ for each concentration were calculated by setting Eq. 4 to zero under consideration that the sum of all components must be 1. On the other hand, the sum of the components, weighted with their fraction of ligands, is the binding degree, and can be written as

$$Bi_c(x_i) \;=\; \mathbf{p}(\infty, x_i)\mathbf{u}_B^T, \tag{5}$$

where $\mathbf{u}_B{}^T$ is the column vector of the fraction of ligands for each model state. In a similar way, we get the normalized fluorescence values of the time courses,

$$F_c(t_j, x_i) \;=\; \alpha_i \mathbf{p}(t_j, x_j)\boldsymbol{u}_B^T, \tag{6}$$

where α_i is an additional factor to normalize the time course to the maximum value at the end of the activation period according to the experimental data $F_m(t_j,x_i)$.

To keep computation time within a reasonable limit, only $n_d = 60$ data points of each time course were chosen (each 30 points for activation and deactivation, respectively). This number of data points was sufficient to fully describe the time courses on the one hand and allowed us to perform global fits in reasonable time on the other.

The χ^2 value computed this way was minimized in the fit procedure. The reduced global $\chi_r{}^2$ value was calculated by dividing χ^2 by the degrees of freedom of the fit

$$\chi_r^2 \;=\; \frac{1}{2n_s - m}\chi^2, \tag{7}$$

where m equals the number of parameters. If only normally distributed random errors contribute to the scattering of the data and if the model fits to the data, then the reduced $\chi_r{}^2$ value should be close to unity. For the best model found in this study, the reduced $\chi_r{}^2$ value was ~2.8.

RESULTS

Ligand binding and unbinding in closed HCN2 channels

To gain insight into the action of the subunits in homotetrameric HCN2 channels, we analyzed the relative steady-state binding of the ligand as well as the kinetics of ligand binding and unbinding (F/F_{max}) by using the fluorescently labeled ligand fcAMP and confocal patch-clamp fluorometry (29,34). In channels preactivated by a hyperpolarizing pulse to −130 mV, a jump from 0 to 7.5 μM fcAMP, a nearly saturating fcAMP concentration, further enhances activation (Fig. 1 *A*). The time course of fcAMP binding is characterized by an initial rapid phase that is followed by a slow phase, resembling the time course of current activation. At this concentration, we previously assumed that all four binding sites are occupied (29). At −30 mV, a jump to 7.5 μM fcAMP generated less relative binding at the steady state than at −130 mV and, as expected, a current was not activated at this subthreshold voltage (Fig. 1 *B*). Comparison of normalized time courses reveals that the characteristic slow phases of binding and unbinding at −130 mV are missing at −30 mV (Fig. 1 *C*), supporting earlier results, which show that this slow phase is kinetically related to channel activation (29).

To explore the processes underlying binding and unbinding at −30 mV more systematically, we performed respective experiments at the five ligand concentrations 0.075, 0.25, 0.75, 2.5, and 7.5 μM fcAMP and averaged between five and seven traces at each concentration (Fig. 2 *A*). Fit of the steady-state concentration-binding relationship with a Hill function (Eq. 1) showed a rightward shift for nonactivated channels at −30 mV (BC_{50} = 2.46 μM fcAMP) compared to activated channels at −130 mV (BC_{50} = 0.61 μM fcAMP) (Fig. 2 *B*). Notably, at −30 mV the Hill coefficient H of 1.28 still exceeded unity although it was slightly below the value of 1.56 determined at −130 mV. This suggests that also in nonactivated HCN2 channels there is cooperativity among the subunits but with lesser intensity than in voltage-activated channels. A Hill coefficient,

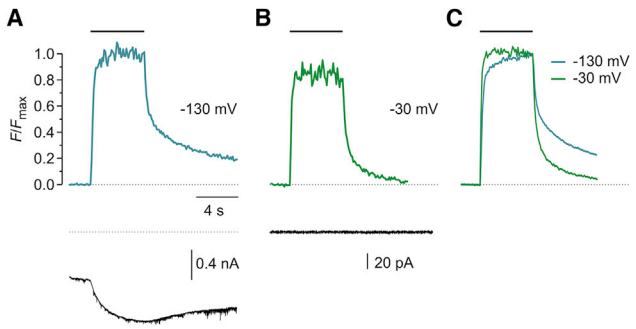

FIGURE 1 Time course of fcAMP binding and unbinding to HCN2 channels. (*A*) Ligand binding and current activation in channels preactivated by a voltage pulse from −30 to −130 mV in a representative patch. Application of fcAMP generated a time course of ligand binding and unbinding that consisted of a rapid and a slow component (*blue trace*, *top*) and an extra current component (*black trace*, *bottom*). The time course for binding (F) was normalized with respect to the steady-state binding at −130 mV and 15 μM fcAMP (F_{max}). (*B*) Respective time course of ligand binding and unbinding for nonactivated channels at −30 mV in a representative patch. In the absence of current activation, fcAMP binding and unbinding are rapid. Same normalization as in (*A*). (*C*) Superimposition of normalized averaged time courses of binding and unbinding at −30 mV (n = 5) and −130 mV (n = 12).

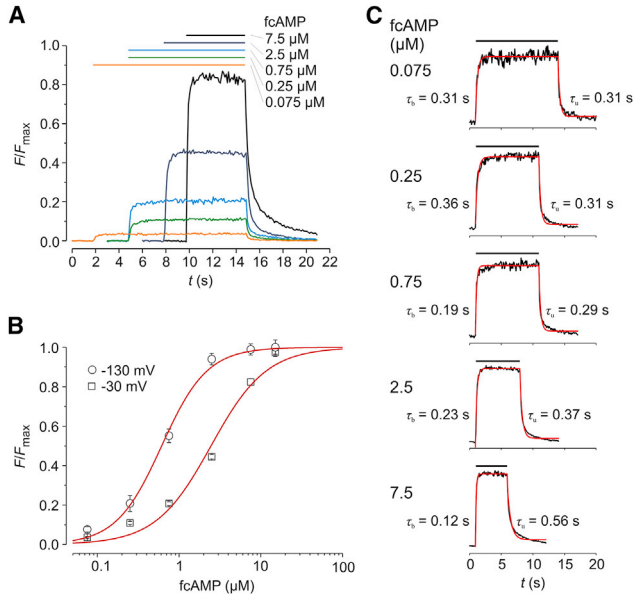

FIGURE 2 Binding of fcAMP to nonactivated HCN2 channels at five concentrations. (*A*) Averaged time courses of binding and unbinding. The number of individual traces, *n*, included in each averaged trace is indicated. Each individual trace was obtained from a different patch. The traces are normalized with respect to the binding at −130 mV and 15 μM fcAMP (F/F_{max}). (*B*) Steady-state concentration-binding relationship at −130 and −30 mV. Fit of the relationships with Eq. 1 (*continuous curves*) yielded −130 mV, BC_{50} = 0.61 μM, and H = 1.56 and −30 mV, BC_{50} = 2.46 μM, and H = 1.28. (*C*) Fit of the time courses (*red curves*) of fcAMP binding and unbinding with a single exponential using Eqs. 2a and 2b, respectively.

however, only provides a guess for the minimum number of subunits involved in a cooperative process but does not provide any further mechanistic insight.

We next quantified the time courses of ligand binding and unbinding at the five fcAMP concentrations by fits with single exponentials, yielding the time constants τ_b and τ_u, respectively (Eqs. 2a and 2b). When comparing τ_b = 0.31 s at 0.075 μM fcAMP with τ_b = 0.19 s at 0.75 μM fcAMP, i.e., a 10-fold different fcAMP concentration, it increases only by a factor of 1.6 (Fig. 2 *C*). This shows that the ligand binding is not rate-limited by the binding process alone but either by the unbinding process or subsequent conformational changes or both. Fig. 2 *C* also shows that the unbinding depends on the ligand concentration only a little, suggesting that in contrast to channels preactivated by voltage (29), nonactivated channels do not trap any ligands, at least up to the fcAMP concentration of 7.5 μM.

The subunits do not operate independently

To gain further insight into the kinetics of the conformational changes in nonactivated channels, we subjected the averaged time courses of ligand binding and unbinding, shown in Fig. 2, *A* and *C*, together with the values of steady-state binding at the five ligand concentrations to a global fit analysis with Markovian models. Assuming as the most simple case that in channels not preactivated by voltage all subunits bind and unbind a ligand independently from each other with first-order kinetics, we fitted a respective C-C model to the data (Fig. 3; model 1 in Table 1).

This model proved to be inadequate as judged by eye and the large value of 15.86 for the reduced χ^2 (χ_r^2), which ideally approximates unity. When adding a conformational change (flip) to a flipped state (C*) following the ligand binding (36), the global fit improved (Fig. 4; model 2 in Table 1). Nevertheless, the fit remained inadequate for part of the time courses and, in particular, for the steady-state concentration-binding relationship at the higher concentrations.

We therefore repeated this approach with a model including two coupled binding steps with a flip from both the mono- and the biliganded state (model 3 in Table 1). Despite a doubling of the free parameters from 4 to 8, the result was that χ_r^2 did not improve; it even deteriorated.

Extending this analysis to models with three binding and respective flip steps led to a notable improvement of χ_r^2. In total 14 such models with between 6 and 9 parameters were tested, including various assumptions for equity or difference of binding and flip steps as well as for a flip of the whole channel or of the individual subunits (Table S1 in the Supporting Material). It turned out that 11 models (models 3-1 to 3-11) with a flip of the whole channel produced lower χ_r^2 values than the three tested models with a flip of the individual subunits (models 3-12 to 3-14),

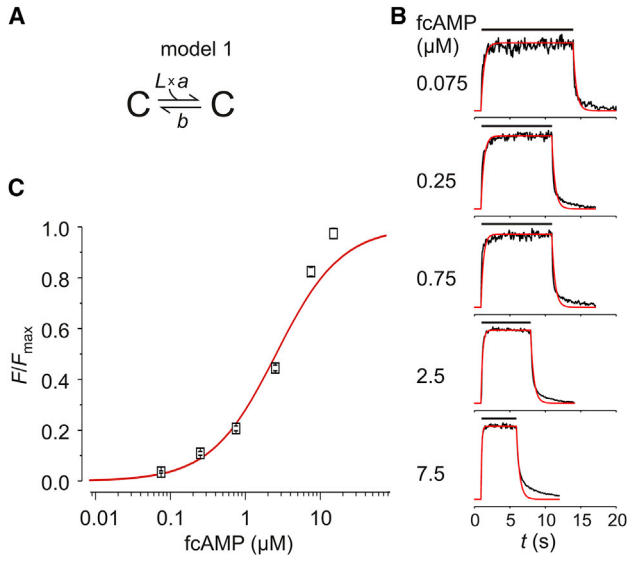

FIGURE 3 Global fit with a C-C model assuming independently operating subunits. (*A*) Scheme of model 1 (Table 1). *L* denotes a ligand. (*B*) Normalized and averaged traces of binding and unbinding at five fcAMP concentrations with superimposed curves (*red*) as best fit. (*C*) Fit of steady-state binding (F/F_{max}) obtained by the same global fit as in (*B*). F_{max} was determined at −130 mV and 15 μM fcAMP. Parameters: $a = 8.58 \times 10^5\ M^{-1}\ s^{-1}$, $b = 2.20\ s^{-1}$, $\chi_r^2 = 15.86$.

TABLE 1 Models fitted by the Global Fit strategy containing 1–4 ligand binding steps

No.	scheme	no. of free parameters	χ_r^2
1		2	15.86
2		4	12.63
3	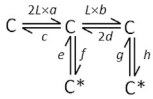	8	21.18
4	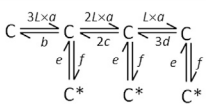	6	3.25
5	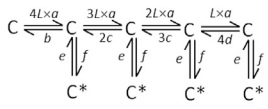	6	2.81

C specifies a closed state of the channel, *C** a flipped state. For simplicity the states are not numbered. *L* is a ligand in a ligand-binding step. Free parameters were the rate constants (*a*,*b*,….). χ_r^2 denotes the reduced χ^2 value. The values of the parameters are provided by Tables S1–S3.

although the latter models belonged to those with the highest number of free parameters. This result supports the idea of a concerted flip of the subunits. Model 4 in Table 1 is the best of the models in Table S2 with respect to the value of χ_r^2. Notably, despite the fact that the number of free parameters was only six, and thus by two less than in model 3, χ_r^2 was markedly smaller. This result suggests that the binding of more than two ligands is of particular relevance for eliciting cooperative effects between the subunits.

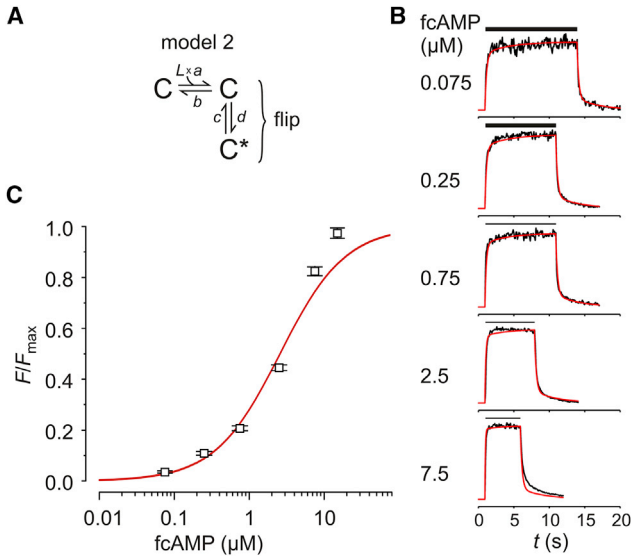

FIGURE 4 Global fit with a model assuming binding and flipping of independent subunits. (*A*) Scheme of the model containing a ligand (*L*) binding step and a subsequent flip of only the same subunit (model 2 in Table 1). (*B* and *C*) Analog to Fig. 3. Parameters: $a = 1.32 \times 10^6\ M^{-1}\ s^{-1}$, $b = 4.00\ s^{-1}$, $c = 3.14 \times 10^{-1}\ s^{-1}$, $d = 5.54 \times 10^{-2} s^{-1}$, and $\chi_r^2 = 12.63$.

In the closed channel, four subunits also cooperate

Because HCN channels are tetramers, it was plausible to also test models with four sequential binding and respective flip steps. In total, 51 such models with between 6 and 11 parameters were tested, again including various assumptions for equity or difference of binding and flip steps as well as for a flip of the whole channel or of the individual subunits (Table S3). Also in the case of four binding steps, a big number of models with a flip of the whole channel produced lower χ_r^2 values (models 4-1 to 4-17) than models with flipping individual subunits (models 4-18, 4-35, 4-46, 4-48). Among those, the models 4-35, 4-46, and 4-48 contained more free parameters than the best 17 models with a concerted flip. But the best way to demonstrate the superiority of models with a concerted flip over models with independently flipping subunits is to compare two models with the same assumptions for the cooperativity and number of free parameters but with a concerted flip on the one hand and independently flipping subunits on the other. This is demonstrated for our favorite model (model 5 in Table 1) and model 4-18 (Table S3). The favorite model 5 (4-1) with a concerted flip produced a significantly lower χ_r^2 value than model 4-18. As an additional control, a model without flip (model 4-42) proved to be poor, although all four rate constants for binding and unbinding were free parameters. Together, these results show that there is a conformational flip and that it is caused by one concerted step of the four subunits but not by independently operating subunits.

A further result was that six models with four binding steps indeed produced still lower χ_r^2 values than the best model with only three sequential binding steps, despite the fact that the number of free parameters was similar or even equal. The best model with respect to χ_r^2 (model 5 in Table 1) produced a χ_r^2 of only 2.81 compared to 3.25 obtained for the best model with three binding steps (model 4 in Table 1). The fit with model 5 is shown in Fig. 5, *A*–*C*. The parameters are provided by Table 2. Because the number of parameters was 6 in both fits, our data directly suggest that liganding of all four subunits is involved in the concerted conformational change of the channel. These results led us to the conclusion that there is cooperativity of the four subunits already in a closed HCN2 channel.

Effect of voltage on the microscopic affinity

Knowledge of the equilibrium association constants K_{A1}–K_{A4} for the closed nonactivated channel according to

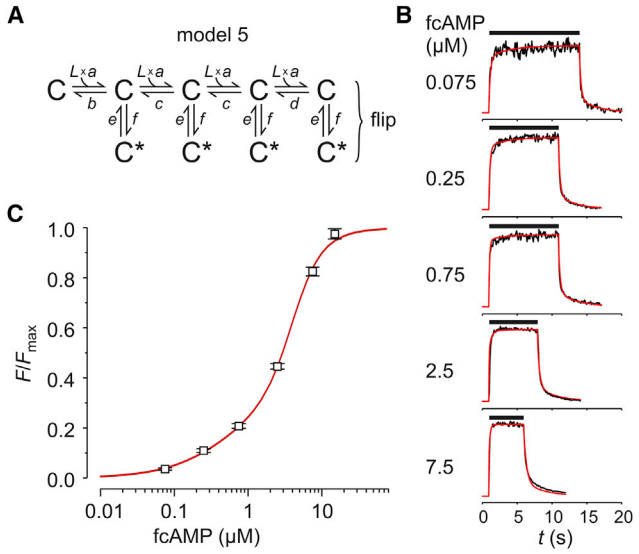

FIGURE 5 Global fit with a model containing four binding steps and one concerted flip. (*A*) Scheme of the model containing four ligand (*L*) binding steps and a concerted flip of all four subunits (model 5 in Table 1). (*B* and *C*) Analog to Fig. 3. The parameters are provided by Table 2.

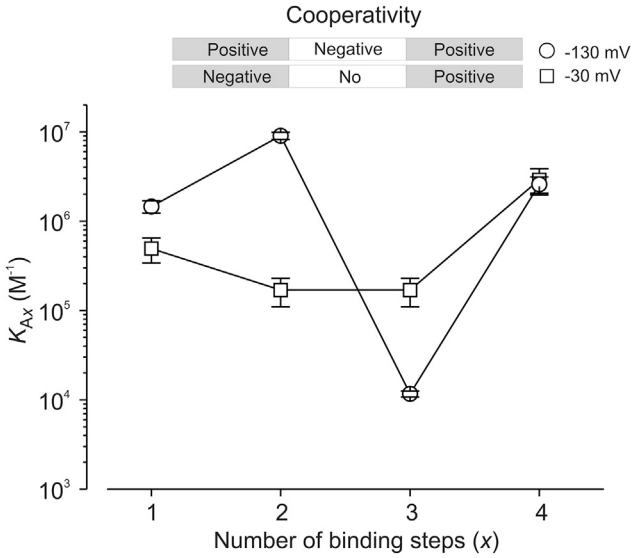

FIGURE 6 Microscopic binding affinity for fcAMP in nonactivated and activated channels. The values of the equilibrium association constants K_{A1}–K_{A4} obtained for model 5 (Table 1) are plotted for nonactivated channels (−30 mV) and activated channels (−130 mV). The values for the activated channels were obtained from a previous study (29). The values for the second and the third binding step at −30 mV were set equal.

model 5 (Table 2) allowed us to relate these constants to those determined for the channel preactivated by a voltage pulse to −130 mV as reported earlier (29) and, thus, to determine the effect of voltage-induced activation on the microscopic binding affinity of the four binding steps (Fig. 6). While K_{A1} and K_{A4} are nearly unaffected by voltage, there is a strong and opposite effect of hyperpolarization-induced activation on K_{A2} and K_{A3}: K_{A2} is by more than an order of magnitude increased whereas K_{A3} is by more than one order of magnitude decreased. Hence, the high energy barrier associated with the third binding step (29) is only inferred by voltage-induced channel activation.

TABLE 2 Rate and equilibrium constants for model 5

	Dimension	Mean	Err%
Rate Constant			
a	$M^{-1}\ s^{-1}$	2.00×10^{6}	15
b	s^{-1}	$4.05 \times 10^{\circ}$	16
c	s^{-1}	1.18×10^{1}	20
d	s^{-1}	6.87×10^{-1}	18
e	s^{-1}	3.51×10^{-1}	22
f	s^{-1}	7.11×10^{-2}	42
Equilibrium Constant			
K_{A1}	M^{-1}	4.94×10^{5}	8
K_{A2}	M^{-1}	1.69×10^{5}	9
K_{A3}	M^{-1}	1.69×10^{5}	9
K_{A4}	M^{-1}	2.91×10^{6}	18
E	–	2.03×10^{-1}	21

The rate constants *a–f* are specified in Fig. 4 *A*. Err% is the relative error (mean ± SE divided by mean in %). K_{A1} through K_{A4} denote the equilibrium association constants of the four binding steps. *E* is the flip equilibrium constant given by *e*/*f*. The errors of the equilibrium constants are calculated using the covariance matrix of the fitted parameters.

DISCUSSION

In this study we measured steady-state and time-dependent ligand binding to functional but closed HCN2 channels and we present evidence that the ligand binding evokes a conformational flip in the channel. We demonstrate that four sequential binding reactions are involved. For the best model with four ligand binding steps and one flip from each ligated state (model 5 in Table 1), we quantified the microscopic affinities and related them to those in channels preactivated by hyperpolarizing voltage as described earlier (29). In addition to this, we determined rate constants for all reactions. Hence, our data provide kinetic information about the molecular mechanism proceeding in nonactivated HCN2 channels when fcAMP binds.

The most prominent effect of channel activation by voltage on the microscopic binding affinity was to increase K_{A2} and to decrease K_{A3}. In other words, the binding of the second ligand is facilitated and that of the third ligand is impeded, generating with respect to the microscopic binding affinity the complex cooperativity pattern "positive-negative-positive" (29,44). In contrast, at −30 mV the respective cooperativity pattern is "negative-no-positive" (Fig. 6). Hence, there is an essential effect of channel activation on the affinity of the binding sites involved in the binding of the second and third ligand. These results further specify earlier results on HCN2 channels showing a reciprocal relationship between channel activation and the binding affinity (34). It should be noted that in the fit of our favorite model 5 (Table 1) we set the rate constants underlying K_{A2} and K_{A3} equal. Despite this simplifying and somewhat arbitrary

assumption, the effect of activation on these two equilibrium association constants (Fig. 6) is viewed to be robust because in channels preactivated by voltage, K_{A2} and K_{A3} differed enormously by three orders of magnitude and no fit could be obtained there when equating K_{A2} and K_{A3}. Furthermore, the errors obtained from the covariance matrix under both conditions are reasonably small (Fig. 6) and thus confirm our interpretation.

Concerning the flip following the ligand binding described herein, our results suggest that it is a concerted flip of all subunits but not of the liganded subunits only. This suggests that a nonactivated channel acts as whole tetramer (24,45) already when the first ligand binds and that this action becomes promoted in proportion to the number of further bound ligands. It is presently not clear whether this action involves only the tetrameric CNBD or also parts of the transmembrane portion of the channel. The question may arise why we did not detect the flipped state in our previous analysis on channels preactivated by a hyperpolarizing voltage pulse to −130 mV (29). We assume that under those conditions the reciprocal feedback from the activated channel pore to the flip of the nonactivating channel considered herein prevented the possibility to identify the flip.

How can the conformational flip be attributed to structural changes in the channels? Recent work in isolated CNBDs provided a guess of the initial conformational changes following the binding of cAMP to the binding site, in which the movement of the C-helix to occlude the cyclic nucleotide in the binding pocket plays a key role (46–48). Other structures have also been proposed to participate, including a folding of the P-helix within the PBC element, a translational movement of the B-helix, and a folding and movement of the F-helix (47). These changes presumably lead to an elimination of steric clashes evoked by the CNBD on the tetrameric C-linker that finally leads to the pore opening (48), at least in channel preactivated by voltage. It is plausible that all these arrangements are included in the conformational flip of nonactivated channels studied herein. However, considerable caution is needed when directly relating the conformational flip to these structural results because our functional data were obtained from whole channels whereas the structural data are from isolated CNBDs only. Hence, in the isolated CNBD the energetic feedback of the transmembrane channel domain on the CNBD (34) is completely missing. As outlined above, it is also possible that rearrangements in the transmembrane domain contribute to the conformational flip studied herein. Moreover, the role of the N-terminus is completely elusive in this context. Hence, the conformational flip studied herein provides information about a global conformational change of the nonactivated channel.

Another result of this study is remarkable: Despite the superiority of models with four binding steps and one concerted flip (model 5 in Table 1; Fig. 5), a model with independently operating subunits, i.e., one binding step and one flip (model 2 in Table 1; Fig. 4), already produced a significantly better description than the C-C model (model 1 in Table 1; Fig. 3). This result supports the notion that, in a nonactivated channel, the flip evoked by the ligand binding to a subunit predominantly affects the binding affinity of this particular subunit (49) and that the interaction between the subunits is of lesser effect.

If relating the results of our modeling to established kinetic models, the concerted (allosteric) conformational flip in the type of models favored herein matches one of the basic assumptions of the MWC-model (31) but does not support the necessity to use more complex models of the Koshland-Nemethy-Filmer type (50). Nevertheless, the model favored herein differs from the MWC model by the nonmonotonous change of the affinity of the four binding reactions.

We finally like to emphasize that the measurements presented in this report are based on measuring the ligand binding and unbinding, and that these data were interpreted by hidden Markov models to substantiate a kinetic scheme describing the binding and gating of the closed channel. This approach is basically opposite to common approaches in electrophysiology, studying channel activation and substantiating hidden Markov models describing ligand binding and the activation gating (51–54). A major aspect of our approach is that it reports other properties of channel gating than those associated with activation. Hence, this approach is applicable to other nonactivated ligand gated channels as well and, most notable, to any other membrane receptors, as, e.g., the huge number of G-protein coupled receptors (55). Moreover, if a readout of conformational changes is included in the experiments, e.g., by evaluating the kinetics of Förster resonance energy transfer (56), the constraints in the fit will grow significantly, thereby enabling kinetic analyses with much greater detail than herein.

SUPPORTING MATERIAL

Three tables are available at http://www.biophysj.org/biophysj/supplemental/S0006-3495(15)01008-5.

AUTHOR CONTRIBUTIONS

S.T. performed the experiments, analyzed the data, and designed the figures; E.S. performed the global fits; J.K. performed experiments and contributed to the data analysis; and K.B. designed the study and wrote the article.

ACKNOWLEDGMENTS

We thank K. Schoknecht, S. Bernhardt, and A. Kolchmeier for excellent technical assistance.

This work was supported by the grants No. BE1250/16-1 and BE1250/16-2 to K.B. as well as No. SFB/TR166, all by the Deutsche Forschungsgemeinschaft.

REFERENCES

1. Gauss, R., R. Seifert, and U. B. Kaupp. 1998. Molecular identification of a hyperpolarization-activated channel in sea urchin sperm. *Nature.* 393:583–587.
2. Ludwig, A., X. Zong, …, M. Biel. 1998. A family of hyperpolarization-activated mammalian cation channels. *Nature.* 393:587–591.
3. Santoro, B., D. T. Liu, …, G. R. Tibbs. 1998. Identification of a gene encoding a hyperpolarization-activated pacemaker channel of brain. *Cell.* 93:717–729.
4. Moosmang, S., J. Stieber, …, A. Ludwig. 2001. Cellular expression and functional characterization of four hyperpolarization-activated pacemaker channels in cardiac and neuronal tissues. *Eur. J. Biochem.* 268:1646–1652.
5. Santoro, B., S. Chen, …, S. A. Siegelbaum. 2000. Molecular and functional heterogeneity of hyperpolarization-activated pacemaker channels in the mouse CNS. *J. Neurosci.* 20:5264–5275.
6. Chan, C. S., R. Shigemoto, …, D. J. Surmeier. 2004. HCN2 and HCN1 channels govern the regularity of autonomous pacemaking and synaptic resetting in globus pallidus neurons. *J. Neurosci.* 24:9921–9932.
7. Banks, M. I., R. A. Pearce, and P. H. Smith. 1993. Hyperpolarization-activated cation current (I_h) in neurons of the medial nucleus of the trapezoid body: voltage-clamp analysis and enhancement by norepinephrine and cAMP suggest a modulatory mechanism in the auditory brain stem. *J. Neurophysiol.* 70:1420–1432.
8. Cuttle, M. F., Z. Rusznák, …, I. D. Forsythe. 2001. Modulation of a presynaptic hyperpolarization-activated cationic current ($I(h)$) at an excitatory synaptic terminal in the rat auditory brainstem. *J. Physiol.* 534:733–744.
9. Ingram, S. L., and J. T. Williams. 1996. Modulation of the hyperpolarization-activated current (I_h) by cyclic nucleotides in guinea-pig primary afferent neurons. *J. Physiol.* 492:97–106.
10. Saitow, F., and S. Konishi. 2000. Excitability increase induced by β-adrenergic receptor-mediated activation of hyperpolarization-activated cation channels in rat cerebellar basket cells. *J. Neurophysiol.* 84:2026–2034.
11. Notomi, T., and R. Shigemoto. 2004. Immunohistochemical localization of Ih channel subunits, HCN1–4, in the rat brain. *J. Comp. Neurol.* 471:241–276.
12. Brown, H. F., D. DiFrancesco, and S. J. Noble. 1979. How does adrenaline accelerate the heart? *Nature.* 280:235–236.
13. Ludwig, A., X. Zong, …, M. Biel. 1999. Two pacemaker channels from human heart with profoundly different activation kinetics. *EMBO J.* 18:2323–2329.
14. Gauss, R., and R. Seifert. 2000. Pacemaker oscillations in heart and brain: a key role for hyperpolarization-activated cation channels. *Chronobiol. Int.* 17:453–469.
15. Biel, M., C. Wahl-Schott, …, X. Zong. 2009. Hyperpolarization-activated cation channels: from genes to function. *Physiol. Rev.* 89:847–885.
16. DiFrancesco, D. 1986. Characterization of single pacemaker channels in cardiac sino-atrial node cells. *Nature.* 324:470–473.
17. Santoro, B., and G. R. Tibbs. 1999. The HCN gene family: molecular basis of the hyperpolarization-activated pacemaker channels. *Ann. N. Y. Acad. Sci.* 868:741–764.
18. DiFrancesco, D. 1999. Dual allosteric modulation of pacemaker (*f*) channels by cAMP and voltage in rabbit SA node. *J. Physiol.* 515:367–376.
19. Wang, J., S. Chen, and S. A. Siegelbaum. 2001. Regulation of hyperpolarization-activated HCN channel gating and cAMP modulation due to interactions of COOH terminus and core transmembrane regions. *J. Gen. Physiol.* 118:237–250.
20. Wang, J., S. Chen, …, S. A. Siegelbaum. 2002. Activity-dependent regulation of HCN pacemaker channels by cyclic AMP: signaling through dynamic allosteric coupling. *Neuron.* 36:451–461.
21. Robinson, R. B., and S. A. Siegelbaum. 2003. Hyperpolarization-activated cation currents: from molecules to physiological function. *Annu. Rev. Physiol.* 65:453–480.
22. Craven, K. B., and W. N. Zagotta. 2006. CNG and HCN channels: two peas, one pod. *Annu. Rev. Physiol.* 68:375–401.
23. Kaupp, U. B., and R. Seifert. 2001. Molecular diversity of pacemaker ion channels. *Annu. Rev. Physiol.* 63:235–257.
24. Zagotta, W. N., N. B. Olivier, …, E. Gouaux. 2003. Structural basis for modulation and agonist specificity of HCN pacemaker channels. *Nature.* 425:200–205.
25. Stieber, J., G. Stöckl, …, F. Hofmann. 2005. Functional expression of the human HCN3 channel. *J. Biol. Chem.* 280:34635–34643.
26. Bruening-Wright, A., F. Elinder, and H. P. Larsson. 2007. Kinetic relationship between the voltage sensor and the activation gate in spHCN channels. *J. Gen. Physiol.* 130:71–81.
27. Ulens, C., and S. A. Siegelbaum. 2003. Regulation of hyperpolarization-activated HCN channels by cAMP through a gating switch in binding domain symmetry. *Neuron.* 40:959–970.
28. Chen, S., J. Wang, …, S. A. Siegelbaum. 2007. Voltage sensor movement and cAMP binding allosterically regulate an inherently voltage-independent closed-open transition in HCN channels. *J. Gen. Physiol.* 129:175–188.
29. Kusch, J., S. Thon, …, K. Benndorf. 2012. How subunits cooperate in cAMP-induced activation of homotetrameric HCN2 channels. *Nat. Chem. Biol.* 8:162–169.
30. Perutz, M. F., A. J. Wilkinson, …, G. G. Dodson. 1998. The stereochemical mechanism of the cooperative effects in hemoglobin revisited. *Annu. Rev. Biophys. Biomol. Struct.* 27:1–34.
31. Monod, J., J. Wyman, and J. P. Changeux. 1965. On the nature of allosteric transitions: a plausible model. *J. Mol. Biol.* 12:88–118.
32. Benndorf, K., J. Kusch, and E. Schulz. 2012. Probability fluxes and transition paths in a Markovian model describing complex subunit cooperativity in HCN2 channels. *PLOS Comput. Biol.* 8:e1002721.
33. Biskup, C., J. Kusch, …, K. Benndorf. 2007. Relating ligand binding to activation gating in CNGA2 channels. *Nature.* 446:440–443.
34. Kusch, J., C. Biskup, …, K. Benndorf. 2010. Interdependence of receptor activation and ligand binding in HCN2 pacemaker channels. *Neuron.* 67:75–85.
35. Wu, S., Z. V. Vysotskaya, …, L. Zhou. 2011. State-dependent cAMP binding to functioning HCN channels studied by patch-clamp fluorometry. *Biophys. J.* 100:1226–1232.
36. Burzomato, V., M. Beato, …, L. G. Sivilotti. 2004. Single-channel behavior of heteromeric $\alpha1\beta$ glycine receptors: an attempt to detect a conformational change before the channel opens. *J. Neurosci.* 24:10924–10940.
37. Lape, R., D. Colquhoun, and L. G. Sivilotti. 2008. On the nature of partial agonism in the nicotinic receptor superfamily. *Nature.* 454:722–727.
38. Thon, S., R. Schmauder, and K. Benndorf. 2013. Elementary functional properties of single HCN2 channels. *Biophys. J.* 105:1581–1589.
39. Jonas, P. 1995. High-speed solution switching using piezo-based micropositioning stages. *In* In Single-Channel Recording. B. Sakmann and E. Neher, editors. Plenum Press, New York, pp. 231–243.
40. Zheng, J., and W. N. Zagotta. 2003. Patch-clamp fluorometry recording of conformational rearrangements of ion channels. *Sci. STKE.* 2003:PL7.
41. Brown, K. M., and J. E. Dennis. 1972. Derivative-free analogues of the Levenberg-Marquardt and Gauss algorithms or nonlinear least squares approximation. *Numer. Math.* 18:289–297.
42. Press, W. H., S. A. Teukolsky, …, B. P. Flannery. 2002. Numerical Recipes in C: The Art of Scientific Computing. Cambridge University Press, Cambridge, UK, p. 685.
43. Colquhoun, D., and A. G. Hawkes. 2009. A Q-Matrix cookbook. *In* Single Channel Recording. B. Sakman and E. Neher, editors. Springer, New York, pp. 589–633.

44. Benndorf, K., S. Thon, and E. Schulz. 2012. Unraveling subunit cooperativity in homotetrameric HCN2 channels. *Biophys. J.* 103:1860–1869.

45. Lolicato, M., M. Nardini, …, A. Moroni. 2011. Tetramerization dynamics of C-terminal domain underlies isoform-specific cAMP gating in hyperpolarization-activated cyclic nucleotide-gated channels. *J. Biol. Chem.* 286:44811–44820.

46. Puljung, M. C., H. A. DeBerg, …, S. Stoll. 2014. Double electron-electron resonance reveals cAMP-induced conformational change in HCN channels. *Proc. Natl. Acad. Sci. USA.* 111:9816–9821.

47. Saponaro, A., S. R. Pauleta, …, A. Moroni. 2014. Structural basis for the mutual antagonism of cAMP and TRIP8b in regulating HCN channel function. *Proc. Natl. Acad. Sci. USA.* 111:14577–14582.

48. Akimoto, M., Z. Zhang, …, G. Melacini. 2014. A mechanism for the auto-inhibition of hyperpolarization-activated cyclic nucleotide-gated (HCN) channel opening and its relief by cAMP. *J. Biol. Chem.* 289:22205–22220.

49. Colquhoun, D. 1998. Binding, gating, affinity and efficacy: the interpretation of structure-activity relationships for agonists and of the effects of mutating receptors. *Br. J. Pharmacol.* 125:924–947.

50. Koshland, D. E., Jr., G. Némethy, and D. Filmer. 1966. Comparison of experimental binding data and theoretical models in proteins containing subunits. *Biochemistry.* 5:365–385.

51. Altomare, C., A. Bucchi, …, D. DiFrancesco. 2001. Integrated allosteric model of voltage gating of HCN channels. *J. Gen. Physiol.* 117:519–532.

52. Nache, V., E. Schulz, …, K. Benndorf. 2005. Activation of olfactory-type cyclic nucleotide-gated channels is highly cooperative. *J. Physiol.* 569:91–102.

53. Zagotta, W. N., T. Hoshi, and R. W. Aldrich. 1994. *Shaker* potassium channel gating. III: Evaluation of kinetic models for activation. *J. Gen. Physiol.* 103:321–362.

54. Maconochie, D. J., and D. E. Knight. 1992. Markov modelling of ensemble current relaxations: bovine adrenal nicotinic receptor currents analysed. *J. Physiol.* 454:155–182.

55. Kobilka, B. K. 2011. Structural insights into adrenergic receptor function and pharmacology. *Trends Pharmacol. Sci.* 32:213–218.

56. Hlavackova, V., U. Zabel, …, M. J. Lohse. 2012. Sequential inter- and intrasubunit rearrangements during activation of dimeric metabotropic glutamate receptor 1. *Sci. Signal.* 5:ra59.